On the Long-Term Stability of Microwave Radiometers Using Noise Diodes for Calibration

Shannon T. Brown, *Member, IEEE*, Shailen Desai, Wenwen Lu, and Alan B. Tanner

***Abstract*—Results are presented from the long-term monitoring and calibration of the National Aeronautics and Space Administration Jason Microwave Radiometer (JMR) on the Jason-1 ocean altimetry satellite and the ground-based Advanced Water Vapor Radiometers (AWVRs) developed for the Cassini Gravity Wave Experiment. Both radiometers retrieve the wet tropospheric path delay (PD) of the atmosphere and use internal noise diodes (NDs) for gain calibration. The JMR is the first radiometer to be flown in space that uses NDs for calibration. External calibration techniques are used to derive a time series of ND brightness for both instruments that is greater than four years. For the JMR, an optimal estimator is used to find the set of calibration coefficients that minimize the root-mean-square difference between the JMR brightness temperatures and the on-Earth hot and cold references. For the AWVR, continuous tip curves are used to derive the ND brightness. For the JMR and AWVR, both of which contain three redundant NDs per channel, it was observed that some NDs were very stable, whereas others experienced jumps and drifts in their effective brightness. Over the four-year time period, the ND stability ranged from 0.2% to 3% among the diodes for both instruments. The presented recalibration methodology demonstrates that long-term calibration stability can be achieved with frequent recalibration of the diodes using external calibration techniques. The JMR PD drift compared to ground truth over the four years since the launch was reduced from 3.9 to −0.01 mm/year with the recalibrated ND time series. The JMR brightness temperature calibration stability is estimated to be 0.25 K over ten days.**

***Index Terms*—Advanced Water Vapor Radiometer (AWVR), calibration, Jason Microwave Radiometer (JMR), Jason-1, microwave radiometer, noise diode (ND), path delay (PD).**

I. Introduction

THE CALIBRATION of microwave radiometers is generally performed by observing the signal from two sources of known temperature to determine the radiometer transfer function from raw counts to antenna temperature, where the transfer function most generally consists of a gain and offset. Most spaceborne imaging radiometers view an external hot target (∼300 K) and cold space (2.7 K) through the feed as they scan, thus calibrating the entire system, with the exception of the reflector [e.g., the Special Sensor Microwave/Imager (SSM/I), the Tropical Rainfall Measuring Mission's Microwave Imager (TMI), and WindSat] [1]–[3]. When instrument design requirements prohibit viewing external targets, an internal switch, which is generally referred to as a Dicke switch, is used to alternately view two stable sources of known temperature. One source is most often a 50-Ω load held at ambient temperature. Several techniques have been used for the second source, but it commonly takes the form of a noise diode (ND) signal of known brightness coupled into the system, especially for ground-based systems. For satellite instruments, a common design is to internally switch between a reference load and an external feed horn that views cold space [e.g., Topex Microwave Radiometer (TMR), Envisat, and European Remote Sensing Satellite Microwave Radiometer]. While NDs are common in ground-based and airborne microwave radiometers, the long-term stability of such devices is not critical since frequent external calibrations can be performed using laboratory techniques (e.g., ambient absorber and LN_2 targets). This is not the case for the Jason Microwave Radiometer (JMR), which is the first radiometer to be flown in space that uses NDs for calibration [5].

The JMR is included on the Jason-1 ocean altimetry satellite, which was launched on December 7, 2001, to measure the wet tropospheric path delay (PD) experienced by the radar altimeter signal. The JMR is nadir pointing and measures the radiometric brightness temperature T_{B} at 18.7, 23.8, and 34.0 GHz. Monitoring the long-term stability of the JMR NDs is essential because instability in the diodes, whether it be drifts or jumps, will translate directly to the wet tropospheric PD measurements and consequently to errors in the sea-surface height measurements. Tracking potential ND drifts are of particular importance since this signal will influence estimates of global sea-level rise, which is currently estimated to be ∼3 mm/year [6].

Another investigation in which long-term radiometer stability is required is ground-based measurements of wet tropospheric PD for the Cassini Gravity Wave Experiment (GWE). The Advanced Water Vapor Radiometer (AWVR), which was developed for this purpose, operates at 22.2, 23.8, and 31.4 GHz and uses NDs for calibration [7]. Two AWVRs named A1 and A2 have been in nearly continuous operation since August 2001 at the NASA Deep Space Network Goldstone site.

This paper presents results of the long-term monitoring and calibration of the JMR and the AWVR. A time series greater than four years of ND brightness estimated from external calibration techniques with the spaceborne JMR and the

Manuscript received May 31, 2006; revised September 1, 2006. The work described in this paper was performed at the Jet Propulsion Laboratory, California Institute of Technology under a contract with the National Aeronautics and Space Administration.

S. T. Brown is with the Microwave Advanced Systems Section, NASA Jet Propulsion Laboratory, Pasadena, CA 91109 USA (e-mail: Shannon.T.Brown@jpl.nasa.gov).

S. Desai and W. Lu are with the Orbit and Radio Metric Systems Group, NASA Jet Propulsion Laboratory, Pasadena, CA 91109 USA.

A. B. Tanner is with the Ground Based Microwave Applications Group, Jet Propulsion Laboratory, Pasadena, CA 91109 USA.

Color versions of one or more of the figures in this paper are available online at http://ieeexplore.ieee.org.

Digital Object Identifier 10.1109/TGRS.2006.888098

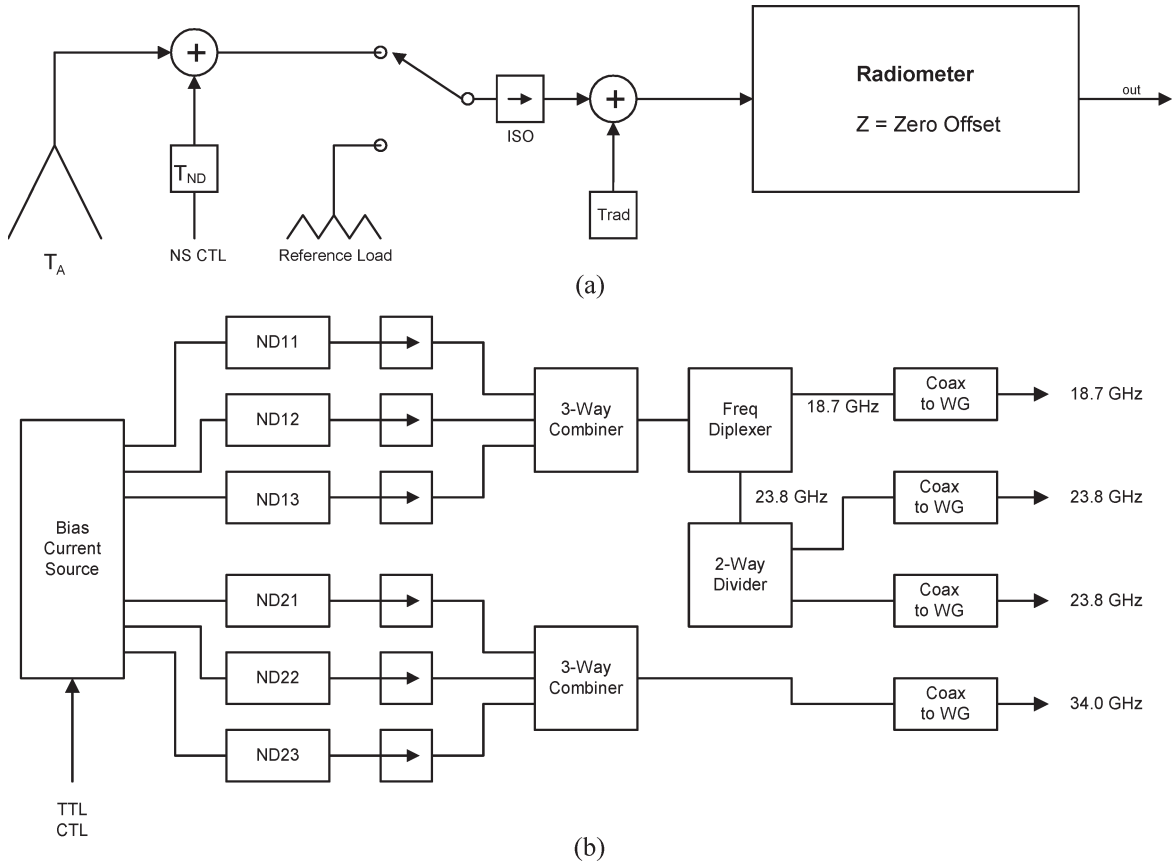

Fig. 1. (a) Simplified JMR radiometer block diagram and (b) ND circuit block diagram.

ground-based AWVRs is presented. The methodology developed for tracking the ND stability of both instruments is presented. A discussion on the possible mechanisms for the observed instability is given in Section VII. The analysis and methodology presented herein can also serve as a reference point for three future NASA spaceborne radiometers that will use NDs for calibration, namely: 1) the Advanced Microwave Radiometer (AMR) on Jason-2 (the follow-on mission to Jason-1); 2) the Aquarius L-band radiometer for measurements of sea-surface salinity [8]; and 3) the Juno Microwave Radiometer for measurements of water vapor abundance in the Jovian atmosphere [9].

II. JMR Calibration Equations

The conversion of raw counts to $T_{\rm B}$ occurs in two processing steps for JMR. The first step, which is performed by Level 1A algorithms, converts the counts to antenna temperatures $T_{\rm A}$, where the gain and offset are estimated using the ND and internal reference load. The second step, which is performed by Level 1B algorithms, converts the antenna temperatures to main beam brightness temperatures using an antenna pattern correction algorithm. A complete discussion of this and other JMR processing algorithms can be found in [5]. This paper focuses solely on the antenna temperature calibration algorithm, which is briefly described in the following.

Because the reference load is internal to the radiometer, the front-end path loss before the Dicke switch must be accounted for in the antenna temperature calibration algorithm. A simplified block diagram of a JMR radiometer chain is shown in Fig. 1(a). The parameterized $T_{\rm A}$ equation is

$$T_{\rm A} = \frac{C_{\rm A} - C_{\rm R}}{C_{\rm ND+A} - C_{\rm A}} T_{\rm ND} + K_{\rm R} T_{\rm Ref} - K_{\rm FH} T_{\rm FH} \quad (1)$$

where $C_{\rm A}$ are the counts with the Dicke switch in the antenna position, $C_{\rm R}$ are the counts with the switch in the reference position, $C_{\rm ND+A}$ are the counts in the antenna position with the ND switched on, $T_{\rm ND}$ is the effective ND brightness temperature, $T_{\rm Ref}$ is the physical temperature of the reference load, $T_{\rm FH}$ is the physical temperature of the feed horn, and $K_{\rm R}$ and $K_{\rm FH}$ are front-end path loss coefficients. $T_{\rm ND}$ is expressed as a quadratic function of its physical temperature $T_{\rm NS}$ referenced to a nominal value T_0, i.e.,

$$T_{\rm ND} = T_{\rm ND0} + \alpha_1 (T_{\rm NS} - T_0) + \alpha_2 (T_{\rm NS} - T_0)^2 \quad (2)$$

where $T_{\rm ND0}$, α_1, and α_2 are the coefficients and $T_{\rm ND}$ is referenced to the antenna aperture. JMR has six NDs, three of which are shared by the 18.7- and 23.8-GHz channels and three that are exclusively for the 34.0-GHz channel. The JMR ND circuit design would not accommodate the use of a single diode across the entire 18.7–34.0-GHz band. A block diagram of the JMR ND circuit is shown in Fig. 1(b). The signal from the three diodes is combined via a three-way power combiner and coupled into the respective channel through a single coaxial-to-waveguide coupler. The 18.7- and 23.8-GHz

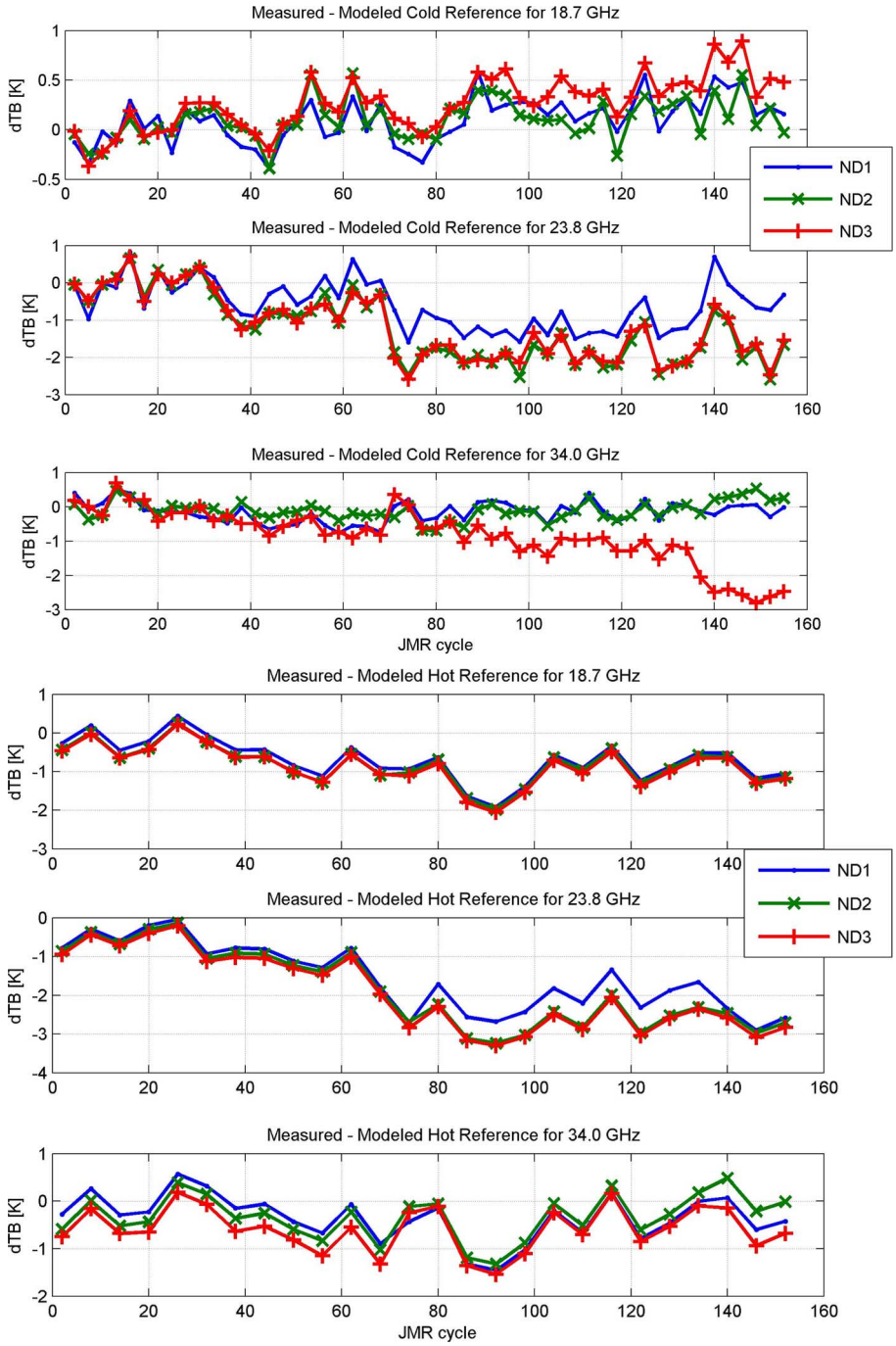

Fig. 2. Deviation of JMR TBs calibrated independently for each ND from on-Earth (top) cold and (bottom) hot references from January 2002 to April 2006. A JMR cycle is roughly ten days.

signals are split after the power combiner using a frequency diplexer. All transmission lines in the ND circuit are rigid microporous Teflon coax. The use of three redundant diodes presents the opportunity to monitor relative changes between the diodes to quickly observe any anomalies, although changes to any components after the three-way power combiner will be common to each diode. The JMR measurement sequence consists of 20 ms in the antenna position and 10 ms in the reference position. The ND signal is switched on via the diode bias for the first 10 ms of each antenna cycle. Each of the three NDs is used for 11 consecutive Dicke cycles (330 ms), resulting in three independently calibrated T_{A} measurements that are then averaged to form the 1-Hz T_{A} measurement. The 1-Hz T_{A} is then passed to the Level 1B processing to generate T_{B}.

The front-end path loss coefficients in (1) account for component losses, impedance mismatches, finite switch isolation, and thermistor biases. An explicit representation of the front-end path loss coefficients in (1) and description of the hardware radiative transfer model used can be found in [4]. The calibration coefficients in (1) and (2) are estimated during prelaunch thermal-vacuum testing but generally require on-orbit fine tuning. A dedicated postlaunch calibration campaign was conducted during the first six months of the mission, at which time the calibration coefficients were adjusted to align the JMR T_{B}s

to on-Earth hot and cold references. It was shown that the JMR PD accuracy at this time exceeded the mission requirement of 1.2-cm rms [5]. Any changes in the hardware in front of the Dicke reference plane (a location just behind the switch, after which any changes are assumed common to the measurements) will result in a change in these derived calibration coefficients and will be evident as errors in the estimated T_{B}.

III. JMR Long-Term Monitoring

A. Brightness Temperatures

We monitor the JMR brightness temperatures using stable on-Earth hot and cold T_{B} references. A vicarious cold reference, which was developed to quantify and remove a drift in the TMR 18.0-GHz channel, is used for the cold end of the T_{B} spectrum [10]. This reference represents a stable statistical lower bound on ocean surface brightness and is ideal for monitoring long-term satellite radiometer calibration in transparent bands. The coldest brightness temperatures at the JMR frequencies occur over the ocean in clear dry atmospheres with calm seas at an optimum sea-surface temperature at which there is a minimum in the product of the emissivity and sea-surface temperature. The theoretical values at 18.7, 23.8, and 34.0 GHz are 125.94, 135.78, and 148.92 K, respectively, with an absolute uncertainty of 1 K, which is defined by the uncertainty in the dielectric constant of sea water.

Pseudoblackbody regions in the Amazon rainforest are used to monitor the T_{B}s at the hot end of the spectrum. A model for the brightness temperature of these regions as a function of frequency, incidence angle, time of day, and time of year was developed by [11]. These two references represent a minimum requirement for monitoring, as the use of a single reference would not allow one to separate gain errors from offset errors. The use of a two-point external calibration requires that the radiometer be assumed linear. Small nonlinearities may exist in radiometer receivers but can be characterized during prelaunch testing and corrected in the software [4].

Fig. 2 shows the deviation of the JMR T_{B}s calibrated independently for each diode from the on-Earth references for the first four years of the mission, from January 2002 to April 2006. A Jason repeat cycle is roughly ten days. The cold reference values have been averaged over 30 days, and the hot reference values have been averaged over 60 days. The hot reference values are averaged over a longer period of time to reduce the scatter in the comparison closer to that of the cold reference, which has a statistical uncertainty of less than 0.2 K at 30 days for JMR. The 18.7-GHz T_{B}s appear to be changing by less than 0.5 K at the cold end and by less than 1 K at the hot end over the four years shown. There are two discrete jumps observed in the 23.8-GHz cold T_{B}s, each of about 1 K, which corresponds to the jumps observed in the PD comparisons around cycles 30 and 70. There is also a jump of about 1.5 K in the 23.8-GHz hot T_{B}'s near cycle 70. The 34.0-GHz ND3 cold T_{B}'s show a drift of about 1 K until cycle 136 when there is a 1.5-K jump observed. The changes observed at the cold end in the 34.0-GHz ND1 and ND2 are less than 1 K. It is the goal of the recalibration methodology to determine the source of the calibration errors and allocate the proper correction to the gain and offset terms in the calibration equations.

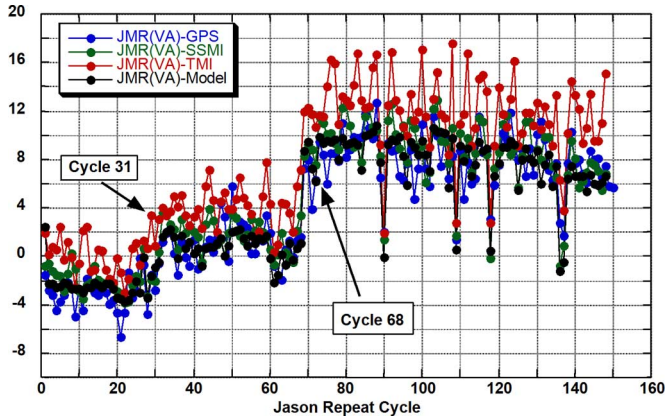

Fig. 3. Ten-day averaged JMR PDs compared to GPS, SSM/I, TMI, and ECMWF from January 2002 to April 2006. The vertical scale is the PD difference expressed in millimeters.

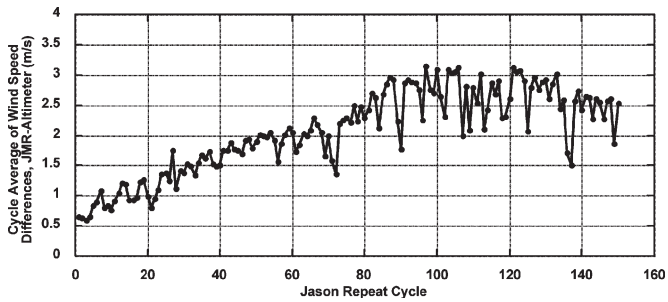

Fig. 4. Ten-day averaged JMR WS estimated differences from altimeters estimate from January 2002 to April 2006.

B. Geophysical Measurements

The calibration changes reflected in the T_{B} comparisons are also evident in comparisons of the derived geophysical measurements to ground truth. This is an important verification since the geophysical ground truth is independent of the on-Earth T_{B} references. For example, if one were to calibrate to potential systematic errors in the on-Earth T_{B} references, it would become readily apparent as errors in the geophysical comparisons. Long-term monitoring, which is subsequent to the postlaunch calibration phase, indicated two shifts in the JMR PD retrieval of about 0.4 cm and an additional 0.8 cm relative to various sources of ground truth 300 and 700 days into the mission, respectively. Ten-day globally averaged differences between JMR PDs and colocated measurements from terrestrial global positioning system (GPS) sites, the European Centre for Medium-Range Weather Forecasts (ECMWF) model, the SSM/I constellation, and the TMI from January 2002 to April 2006 are shown in Fig. 3. The approach used to derive these comparisons is described in [12] and [13].

An intermediate product of the PD algorithm is a measurement of the near-surface wind speed (WS) over the ocean. Ten-day averages of the differences between the WS measurements from the JMR and the altimeter onboard Jason are shown in Fig. 4. A monotonic drift is evident over the first 800 days of

the mission (note that the altimeter measurements of WS show no drift compared to those from the ECMWF model). The T_{B} comparisons and the relative weighting of each in the PD and WS algorithms, respectively, suggest that the changes in the 23.8-GHz channel calibration are mostly responsible for the PD jumps, while a combination of the drifts in the 18.7- and 34.0-GHz channels is mostly responsible for the WS drift.

C. Relative ND Behavior

The relative JMR ND behavior over time is observed by bootstrapping the calibration from diode i to diode j and taking the difference from the value given by (2)

$$\Delta T_{\mathrm{ND}}^{j} = \frac{C_{\mathrm{ND+A}}^{j} - C_{\mathrm{A}}^{j}}{C_{\mathrm{ND+A}}^{i} - C_{\mathrm{A}}^{i}} T_{\mathrm{ND}}^{i}(qT_{\mathrm{NS}}) - T_{\mathrm{ND}}^{j}(T_{\mathrm{NS}}) \ \text{[in Kelvin]}. \tag{3}$$

If the diodes are perfectly stable, then $\Delta T_{\mathrm{ND}}^{j}$ will be a constant. If either diode i or j changes, then $\Delta T_{\mathrm{ND}}^{j}$ will vary. Equation (3) is useful only for determining relative changes among the diodes. An independent reference is required to determine the absolute magnitude of any changes observed between the diodes. Fig. 5 shows the value of (3) for the six possible combinations among the three diodes for each channel at $T_{\mathrm{NS}} = 288.5 \pm 1.0$ K. $\Delta T_{\mathrm{ND}}^{j}$ is evaluated once per second using the 3-Hz ND cycles. These values are then averaged over an orbit (approximately 2 h). The full dynamic range of on-orbit T_{NS} is 285–298 K, with most of the values centered near 288 K. A plot of the noise source physical temperature T_{NS} from January 2002 to February 2006 is shown in Fig. 6. The temperature range is kept small for this analysis to minimize potential errors in the ND temperature correction (i.e., errors in α_1 and α_2) showing up in $\Delta T_{\mathrm{ND}}^{j}$. The linearized temperature coefficient (α_1) is relatively low for the diodes, near 0.04 K/K for the 18.7- and 23.8-GHz diodes, and approximately 0.2 K/K for the 34.0-GHz diodes. The nominal effective brightness of the diodes T_{ND0} is between 90 and 200 K. It is evident from these plots that there exist relative changes among the diodes, on the order of 1%–2% in T_{ND0}, over the first four years of the mission.

IV. JMR Recalibration Methodology

It is apparent from the T_{B}, PD, WS, and relative ND comparisons that a series of time-dependent calibration coefficients is required to recalibrate the JMR. To facilitate this, an optimal estimation-based calibration system is developed to find that set of calibration coefficients, which minimize the rms difference between the JMR T_{B}s and the on-Earth hot and cold absolute T_{B} references discussed in Section III-A. This technique employs, in an optimal way, the same methodology used during the initial on-orbit calibration/validation. The optimal estimator is used [14], i.e.,

$$\vec{x}^{(k+1)} = \vec{x}^{(k)} - \left[S_{\mathrm{a}}^{-1} + J^{T} S_{\varepsilon}^{-1} J\right]^{-1} \times \left[J^{T} S_{\varepsilon}^{-1} \left(\vec{y} - F\left(\vec{x}^{(k)}\right)\right) - S_{\mathrm{a}}^{-1}\left(\vec{x}^{(k)} - \vec{x}_{\mathrm{a}}\right)\right] \tag{4}$$

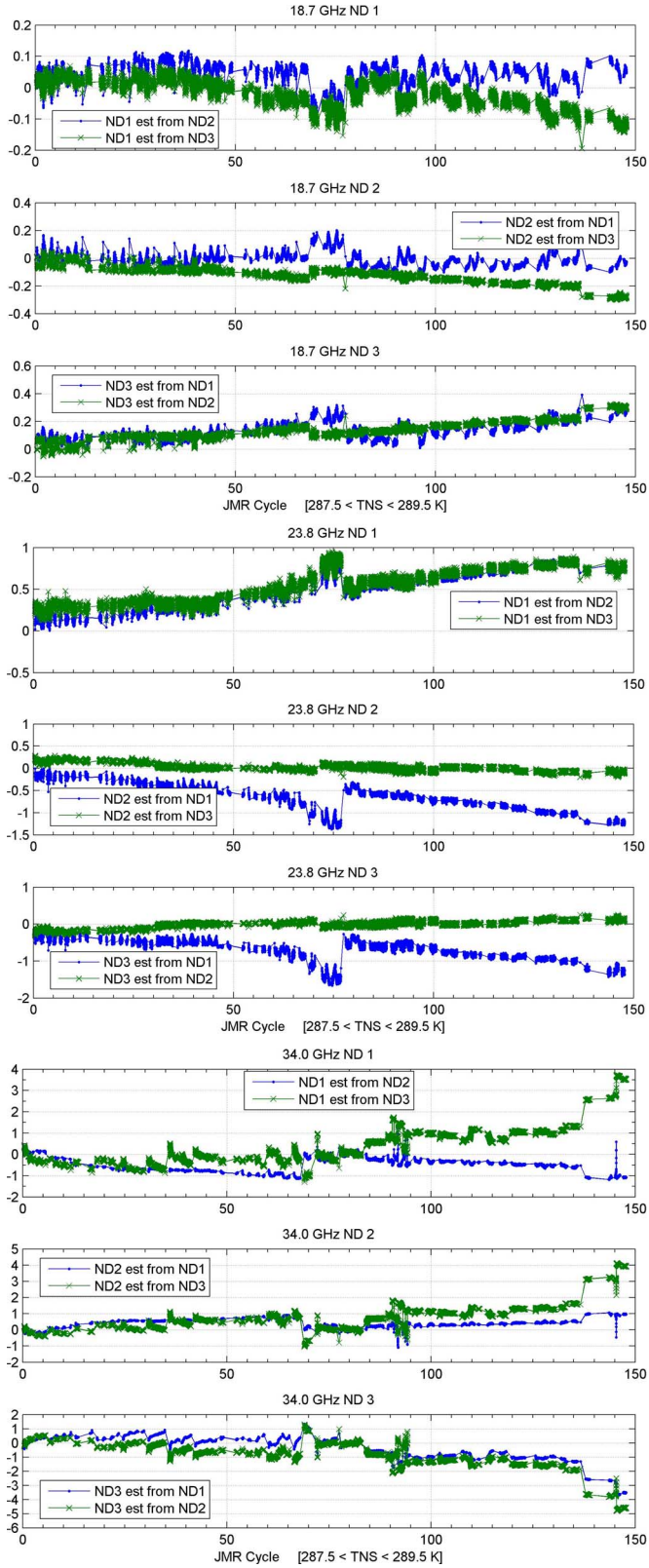

Fig. 5. Relative JMR ND changes [$\Delta T_{\mathrm{ND}}^{j}$ in (3)] for (top) the 18.7-, (middle) 23.8-, and (bottom) 34.0-GHz channels. These plots are for a physical ND temperature of 288.5 + 1.0 K. The ordinate is expressed in Kelvin.

where $\vec{x}$ is the vector of calibration coefficients to be tuned, $\vec{x}_{\mathrm{a}}$ is the *a priori* vector of calibration coefficients (e.g., prelaunch values, postlaunch values, etc.), $\vec{y}$ is the vector of on-Earth

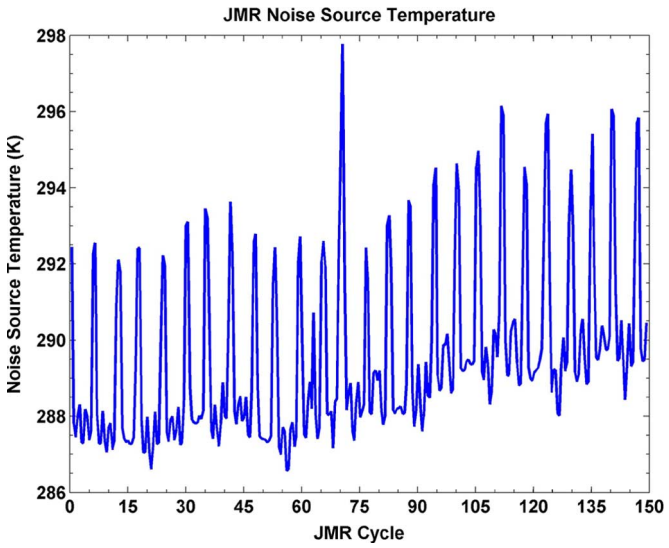

Fig. 6. JMR noise source physical temperature from January 2002 to February 2006.

T_{B} references, S_{ε} is the error covariance matrix for the T_{B} references, and S_{a} is the error covariance matrix for the *a priori* coefficients. $F(\vec{x}^{(k)})$ is the forward model, representing the calibration algorithms, which convert the raw counts to brightness temperatures using the kth realization of the calibration coefficients. In (4), the forward model also includes the algorithms that process the data for comparison to the on-Earth references (i.e., filtering, averaging, etc.). J is the Jacobian of the forward model, which is calculated numerically.

The *a priori* calibration coefficients can be taken initially as the prelaunch values, and their respective uncertainties can be used to form the *a priori* error covariance matrix. The uncertainty on the prelaunch calibration coefficients is calculated as part of the multilinear regression used to derive them from the thermal-vacuum test data (see [4]). This is applicable to the initial postlaunch calibration, after which the fine-tuned calibration coefficients should be used. When generating time-dependent coefficients, assuming that the system is initially calibrated, it is reasonable to set the *a priori* value to the most recent set, i.e., the calibration coefficients determined for the time period previous to the current one. The *a priori* error covariance in this case is given as a representation of the stability of a given coefficient (i.e., how much the coefficient is expected to vary between the times in which it is estimated) and acts to smooth the retrieved coefficient time series. The stability term will be dependent on the system and can be estimated from the time series of the on-Earth reference observations. It was observed that using the *a priori* covariance matrix as a smoothing function reduced the noise in the retrieved coefficient time series and did not change the overall trend (i.e., smooth over or reduce the magnitude of a coefficient jump).

The T_{B} reference vector should include, at minimum, a hot reference and a cold reference to constrain the gain and offset terms in the calibration algorithms. The vicarious cold reference and Amazon rainforest regions, which were discussed in Section III-A, are used to calibrate the T_{B}s. These references are equivalent to those used during the initial JMR postlaunch calibration/validation. The fidelity with which the calibration coefficients can be estimated is directly proportional to the uncertainty of the on-Earth calibration references. Because both references are statistical in nature, the uncertainty of the reference decreases as the data volume increases, barring any systematic errors, such as seasonal or climatic dependence that is not properly accounted for. Errors due to climatic variations are not expected to be appreciable over the four-year timescale presented in this paper, and the seasonal dependencies have been characterized in [10] and [11]. Climatic variations may occur on longer timescales and in the presence of a strong El Nino/La Nina. For example, the brightness of the Amazon region appears to increase by 0.5 K during the 1997–1998 event [17]. Regardless, this will be independently validated by revisiting the geophysical comparisons. It should be noted that the uncertainty discussed here is the relative uncertainty or repeatability of the reference. The absolute value of the references is tied to a theoretical model and subject to the uncertainties therein. This is discussed in detail in [5]. For JMR, the uncertainty of the cold reference at 18.7 and 34.0 GHz is approximately 0.5 K when sampled every three days and 0.1 K when sampled every 30 days (approximately 2.6 million samples). The uncertainty at 23.8 GHz is roughly double these numbers because the cold-reference condition occurs less frequently near the water vapor absorption line. Because the JMR is in a ten-day exact repeat orbit and nonscanning, there are only a limited number of observations over the Amazon rain forest regions within this repeat period. Because of this, the uncertainty in the hot reference is approximately 1.5 K when sampled every ten days and about 1 K when sampled every 30 days. The measurement error covariance matrix is formed assuming that the hot and cold reference errors are uncorrelated and that the 30-day uncertainty values are used to form the diagonal. The uncertainty in the T_{ND0} estimate will be almost equivalent to the uncertainty in the cold reference, due to the lever-armlike nature of this coefficient on the calibration.

The instrument temperature of the radiometer components varies over an orbit and over the various beta angles of the satellite (angle between the orbit plane and a line from the Earth to the Sun). The feed horn experiences a temperature variation of about 15 K over a 60-day period corresponding to the satellite's yaw state, whereas the reference load experiences a 6-K variation. The hot and cold references are sampled over the many instrument temperature states forming multiple independent realizations. In addition to minimizing the rms difference between the JMR T_{B}'s and the on-Earth references, a further constraint is placed on the coefficients to minimize the slope of the T_{B} reference error with respect to instrument temperature by including the slope of the error over temperature as an additional variable to be minimized.

V. JMR Recalibration Results

A. Derived JMR T_{ND0} Time Series

An initial optimization was performed on the nominal ND brightness only, which is T_{ND0} in (2), to assess whether the observed calibration changes could be fully explained by variations in the ND brightness. The front-end loss coefficients are assumed constant with time and are set equal to those derived

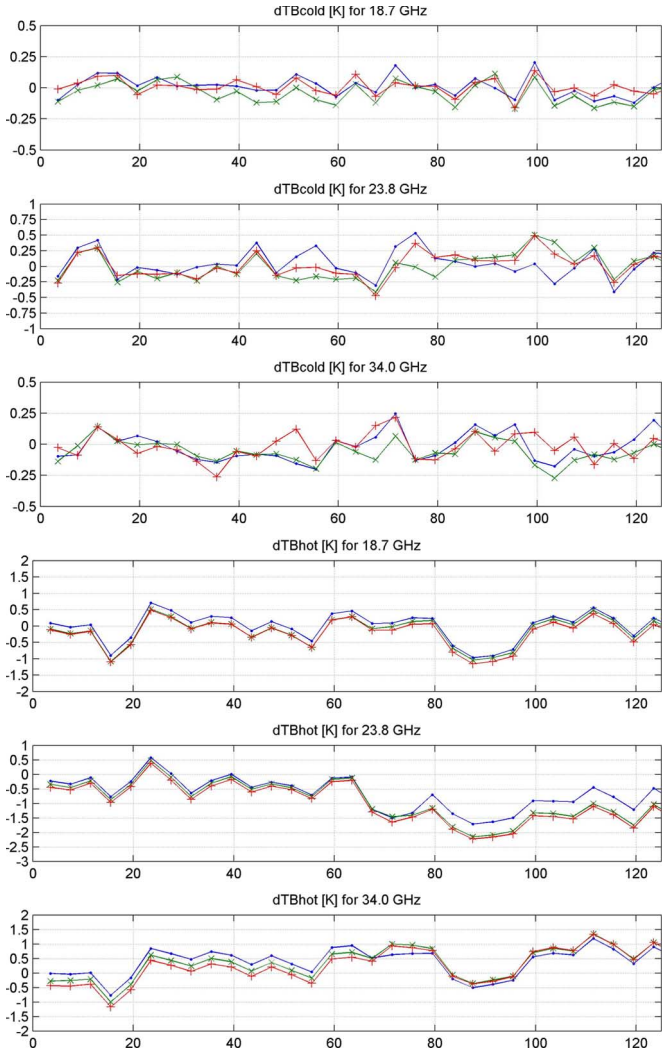

Fig. 7. JMR TB–Reference TB (upper: cold; lower: hot) versus the JMR cycle for (top) 18.7, (middle) 23.8, and (bottom) 34.0 GHz. Optimization was performed on T_{ND0} only.

from the first 300 days of the mission using the calibration software. The optimization software is used to estimate T_{ND0} every 25 days. The JMR T_{B} minus reference T_{B} vector is computed every five days within the 25-day block, and the algorithm finds the set of coefficients that minimize the rms error of these five points at the hot and cold ends. Because T_{ND0} is a gain term, affecting the cold end of the calibration much more than the hot end, optimizing T_{ND0} will essentially minimize the difference between the JMR T_{B}'s and the vicarious cold reference without regard to the hot reference. Fig. 7 shows the difference between the JMR T_{B}'s and the hot and cold T_{B} references for this retrieval at each frequency. The rms difference for the cold T_{B}'s is low for each channel over the four-year time period. There is a shift in the hot reference for the 23.8-GHz channel at the time of the second calibration shift (cycle 70). This indicates that the 23.8-GHz NDs are not entirely responsible for the second calibration shift and that an offset term must be adjusted to minimize the error for the hottest T_{B}s. Tables I(a) and II(a) give the JMR hot reference and cold reference average for each channel before and after cycle 70 with only T_{ND0} optimized. Based on these results, it is determined that adjusting T_{ND0} only for the 18.7-GHz channel is appropriate, but both T_{ND0} and an offset term should be adjusted for the 23.8- and 34.0-GHz channels.

TABLE I
(a) JMR HOT REFERENCE BEFORE AND AFTER CYCLE 70 WITH T_{ND0} OPTIMIZED. (b) JMR HOT REFERENCE BEFORE AND AFTER CYCLE 70 WITH T_{ND0} AND K_{R} OPTIMIZED

(a)

Channel	Before cycle 70	After cycle 70	Difference
18.7 GHz	286.52 K	286.55 K	0.03 K
23.8 GHz	285.99 K	284.84 K	-1.15 K
34.0 GHz	283.79 K	284.39 K	0.6 K

(b)

Channel	Before cycle 70	After cycle 70	Difference
18.7 GHz	286.62 K	286.5 K	-0.07 K
23.8 GHz	286.67 K	286.62 K	-0.05 K
34.0 GHz	284.01 K	283.81 K	-0.2 K

TABLE II
(a) JMR COLD REFERENCE BEFORE AND AFTER CYCLE 70 WITH T_{ND0} OPTIMIZED. (b) JMR COLD REFERENCE BEFORE AND AFTER CYCLE 70 WITH T_{ND0} AND K_{R} OPTIMIZED

(a)

Channel	Before cycle 70	After cycle 70	Difference
18.7 GHz	125.93 K	125.93 K	0.00 K
23.8 GHz	135.74 K	135.78 K	0.04 K
34.0 GHz	148.68 K	148.67 K	-0.01 K

(b)

Channel	Before cycle 70	After cycle 70	Difference
18.7 GHz	125.93 K	125.93 K	0.00 K
23.8 GHz	135.76 K	135.66 K	0.1 K
34.0 GHz	148.67 K	148.67 K	0.00 K

The offset terms in (1) are the K_{R} and K_{FH} coefficients. These coefficients account for the front-end ohmic loss, Dicke switch isolation, reflections among the components, and thermistors biases. A change in any one or a combination of these characteristics could introduce a change in one or both of the front-end path loss coefficients. On-orbit, there are not enough constraints to individually isolate the source of the change, and we therefore choose to apply no constraints on the relationship between the front-end path loss coefficients and hence independently tune them. Ideally, it is preferred to estimate simultaneously K_{R} and K_{FH} as a function of time along with T_{ND0}, but it was found that there are not enough constraints on the retrieval, and only a single offset term should be estimated over time. This is due to the high correlation between the front-end component temperatures and the relatively narrow on-orbit range. A second optimization is performed to estimate a time series of T_{ND0} and K_{R} simultaneously for the 23.8- and 34.0-GHz channels. K_{R} is adjusted instead of K_{FH} due to the smaller on-orbit range of T_{Ref} compared to T_{FH} to minimize the potential for uncertainty on the retrieved coefficient

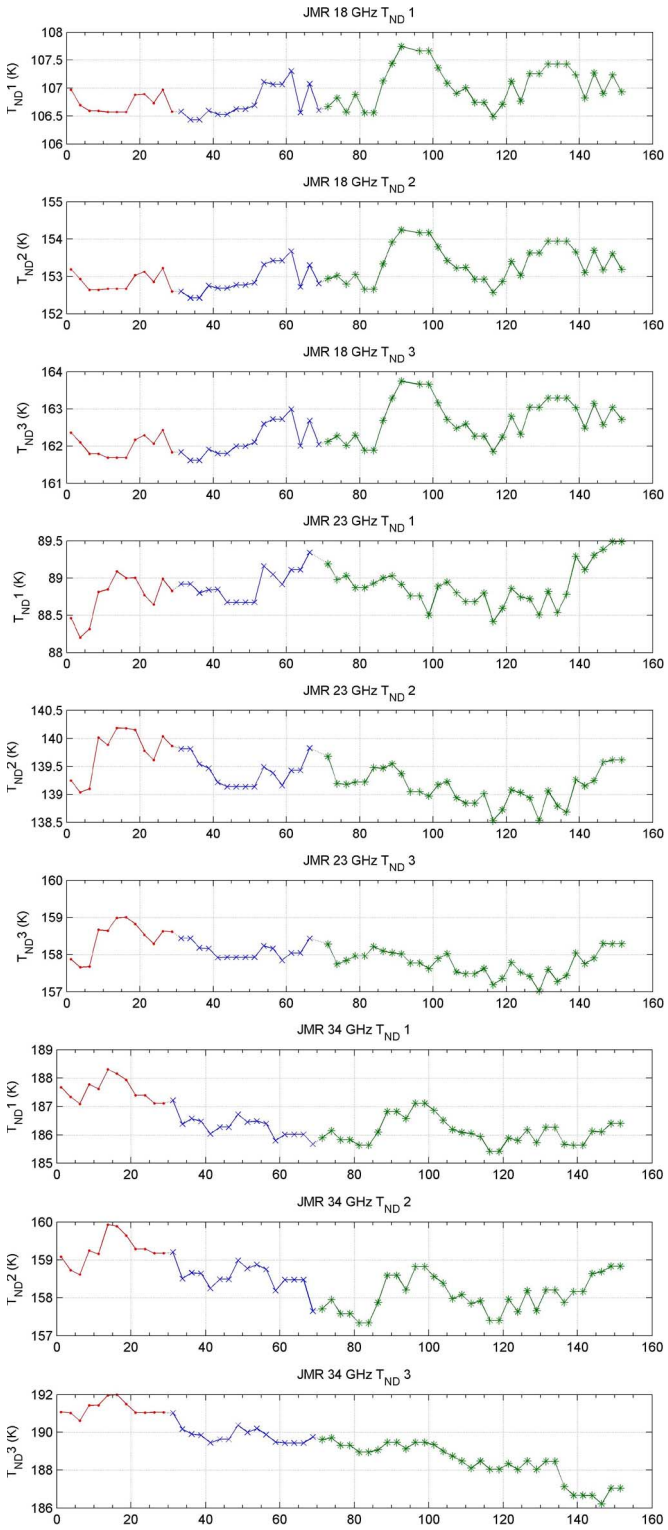

Fig. 8. JMR (top) 18.7, (middle) 23.8, and (bottom) 34.0 GHz T_{ND0} versus the JMR cycle. Optimization was performed on T_{ND0} and K_{R} for the 23.8- and 34.0-GHz channels.

introducing a temperature-dependent error. The retrieved T_{ND0} time series is shown in Fig. 8 for the 18.7-, 23.8-, and 34.0-GHz channels. The retrieved K_{R} for the 23.8- and 34.0-GHz channels is shown in Fig. 9. K_{R} is assumed constant for the 18.7-GHz channel. As shown in Figs. 8 and 9, the calibration shift in the 23.8-GHz channel after cycle 70 is

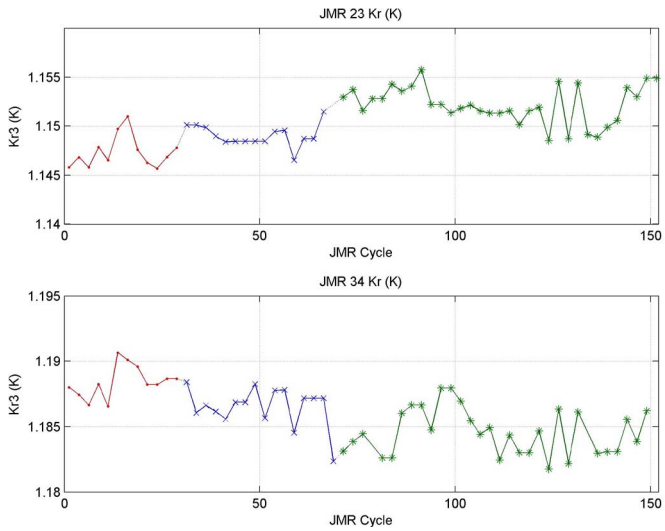

Fig. 9. JMR (top) 23.8 and (bottom) 34.0 GHz K_{R} versus the JMR cycle.

accounted for by a shift in the K_{R} coefficient. The calibration shift after cycle 30 appears to be caused by a decrease of about 0.75 K in the 23.8-GHz ND2 and ND3 brightness. Large drifts appear in the 34.0-GHz NDs. For example, the 34.0-GHz ND3 drifts by approximately 3 K or 1.6% from its initial value, until cycle 136 when it drops by 2 K after an instrument safehold event. The 18.7-GHz NDs change comparatively little: only a few tenths of a Kelvin in the first four years of the mission. Simultaneously adjusting T_{ND0} and K_{R} has minimized the differences in the hot reference before and after cycle 70 that were present when only T_{ND0} was adjusted (Table I). These values are shown in Tables I(b) and II(b). The results for the T_{ND0} and K_{R} optimization at 18.7 GHz are also included in Tables I(b) and II(b) for completeness, and as shown, there is little change from the case where K_{R} is held constant. The hot reference difference is now -0.05 K at 23.8 GHz and -0.20 K at 34.0 GHz, compared to -1.15 K and 0.6 K before.

B. Validation

The validity of the retrieved T_{ND0} time series is first assessed by observing the recalibrated PD and WS comparisons. The calibration coefficients, which were estimated every 25 days, are linearly interpolated to the start time of each JMR cycle and assumed constant for each cycle. The JMR processing algorithms are then used to output the recalibrated geophysical products. The discrete 0.4-cm and additional 0.8-cm PD jumps and WS drifts should be eliminated with the updated calibration. This is shown in Figs. 10 and 11, which are similar to Figs. 3 and 4, except that the JMR measurements of PD and WS are now derived from the recalibrated coefficients. Overall, the retrieval algorithm does a good job of removing the large drifts and jumps in the PD and WS comparisons. The slope of the PD difference over the four-year time period for the recalibrated product is -0.01 ± 0.83 mm/year, compared to 3.9 mm/year before recalibration. This indicates that the long-term drift has been removed through the recalibration methodology. The recalibration does appear to be introducing some additional noise in the PD comparisons on short timescales at the expense of removing the long-term trends. The peak magnitude of this

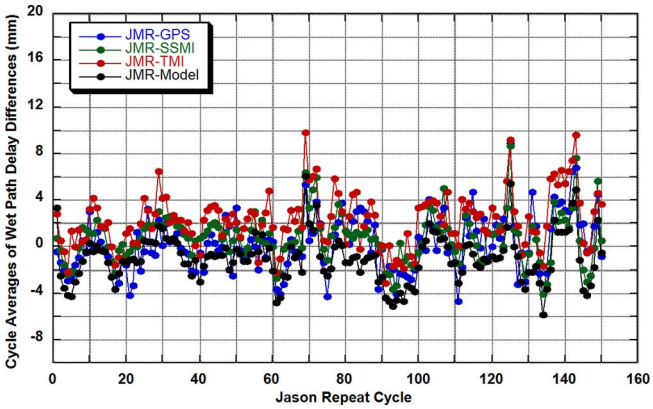

Fig. 10. Ten-day averaged recalibrated JMR PDs compared to GPS, SSM/I, TMI, and ECMWF from January 2002 to April 2005.

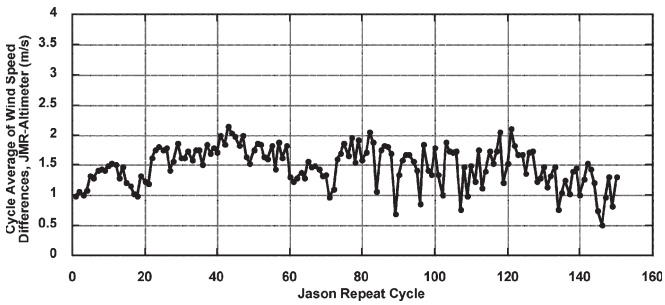

Fig. 11. Ten-day averaged JMR recalibrated WS compared to altimeter-derived WS.

additional noise is in the range of 3–4 mm (see, e.g., times near cycles 90 and 140). The standard deviation of the ten-day averaged differences between JMR and ECMWF is 1.95 mm, compared to 5.5 mm before. If this error is wholly attributed to JMR instability, then it can be used to estimate an upper bound on the recalibrated $T_{\rm B}$ stability at ten days. If calibration errors are assumed to be uncorrelated among the channels, which is reasonable because the coefficient retrieval procedure will tend to randomize the errors between the channels, then the PD error is given by the root sum square of the global PD algorithm, i.e.,

$$\Delta\text{PD} = \left\{(4.1 \times \Delta T_{\text{B18.7}})^2 + (6.5 \times \Delta T_{\text{B23.8}})^2 + (1.9 \times \Delta T_{\text{B34.0}})^2\right\}^{1/2} \quad (5)$$

where the coefficients are expressed in millimeters per Kelvin. Assuming equal errors among the channels, a 1.95-mm PD error translates to a 0.25-K calibration error for the ten-day averaging period.

The T_{ND0} time series should also eliminate the relative drifts between the diodes shown in Fig. 5. Fig. 12 shows ΔT_{ND}^j for the 18.7-, 23.8-, and 34.0-GHz diodes with the T_{ND0} time series used in place of the static coefficient. The plots are shown on the same scale as Fig. 5 for ease of comparison. It can be seen that the retrieved time series does significantly reduce the relative changes among the diodes. Table III shows the rms of ΔT_{ND}^j before and after recalibration. The relative instability among the diodes has been reduced to better than 0.2 K for all diodes.

VI. AWVR ND Stability

Two AWVR units A1 and A2 were developed to estimate the wet tropospheric PD in support of the Cassini GWE. The requirement on the AWVR is that it maintain a 0.01-K calibration stability in $T_{\rm B}$ on timescales of in the range of 1000–10 000 s. The AWVR design is similar to that of the JMR, in that it is a Dicke radiometer, which uses three redundant internal NDs for calibration. Each unit has only three diodes, which are shared among the channels. A simplified block diagram of the AWVR in its temperature enclosure is shown in Fig. 13. One notable difference between the JMR and AWVR designs is that in the AWVR design, the three ND circuits are independent and coupled behind the Dicke switch via three cross-guide couplers. Laboratory experience shows that small changes in reflections among components in the ND circuit are more likely to induce a change in ND brightness than a change in the diode itself; thus, completely independent coupling of redundant diodes is viewed as a better design in monitoring relative ND changes [15]. To meet the stability requirements, the radiometer is kept under precise temperature and humidity control. The temperature of the RF components is kept stable at ± 0.004 °C using a thermal electric controller and double insulation. This environment is contrary to the environment of the JMR diodes that are continually undergoing thermal cycling. A complete system description is found in [7].

The AWVR calibration is accomplished in a similar manner to the JMR. The antenna temperature is determined from (1), with $K_{\rm R} = 1$ and $K_{\rm FH} = 0$. $K_{\rm FH}$ can be set to zero in the case of the AWVR because the front end is isothermal and temperature controlled, meaning the distributed front-end path loss reduces to a single term. The effective brightness of the NDs, which was used to monitor short-term gain fluctuations, is recalibrated on a once-per-month basis using continuous tip-curve calibrations (this well-established calibration procedure is outlined in [16]). For most atmospheric conditions, a full day of continuous tip curves produces an ND estimate to the 0.3-K level or $\sim$0.06%. The tip-curve procedure, which relies on the assumption of a horizontally homogeneous atmosphere, will have the largest uncertainty in humid highly variable conditions. Given the desert location of the AWVRs and the nature of water vapor in the atmosphere, the uncertainty in the tip-curve procedure is limited to the shorter timescales and is not expected to introduce systematic errors in the long-term ND trends. No temperature correction is necessary for the diode brightness because of the temperature controller. Analysis of the AWVR $T_{\rm B}$s shows that the calibration stability requirement is met for all channels, with some channels reaching 0.003-K stability over 10 000-s timescales. The stability on monthly timescales is estimated to be better than 0.08 K [7]. This suggests that the AWVR NDs are extremely stable on timescales of less than one month. To investigate the long-term stability, the ND estimates derived from the continuous tip curves were combined for greater than four years of operating time. The derived brightness of the diodes estimated from daily tip curves and then averaged over five days is shown in Fig. 14 for each channel of AWVR A1 for the time period of August 2001–July 2005. Data gaps are present when the radiometer was not operating. An equivalent set of plots for the A2 radiometer is shown in

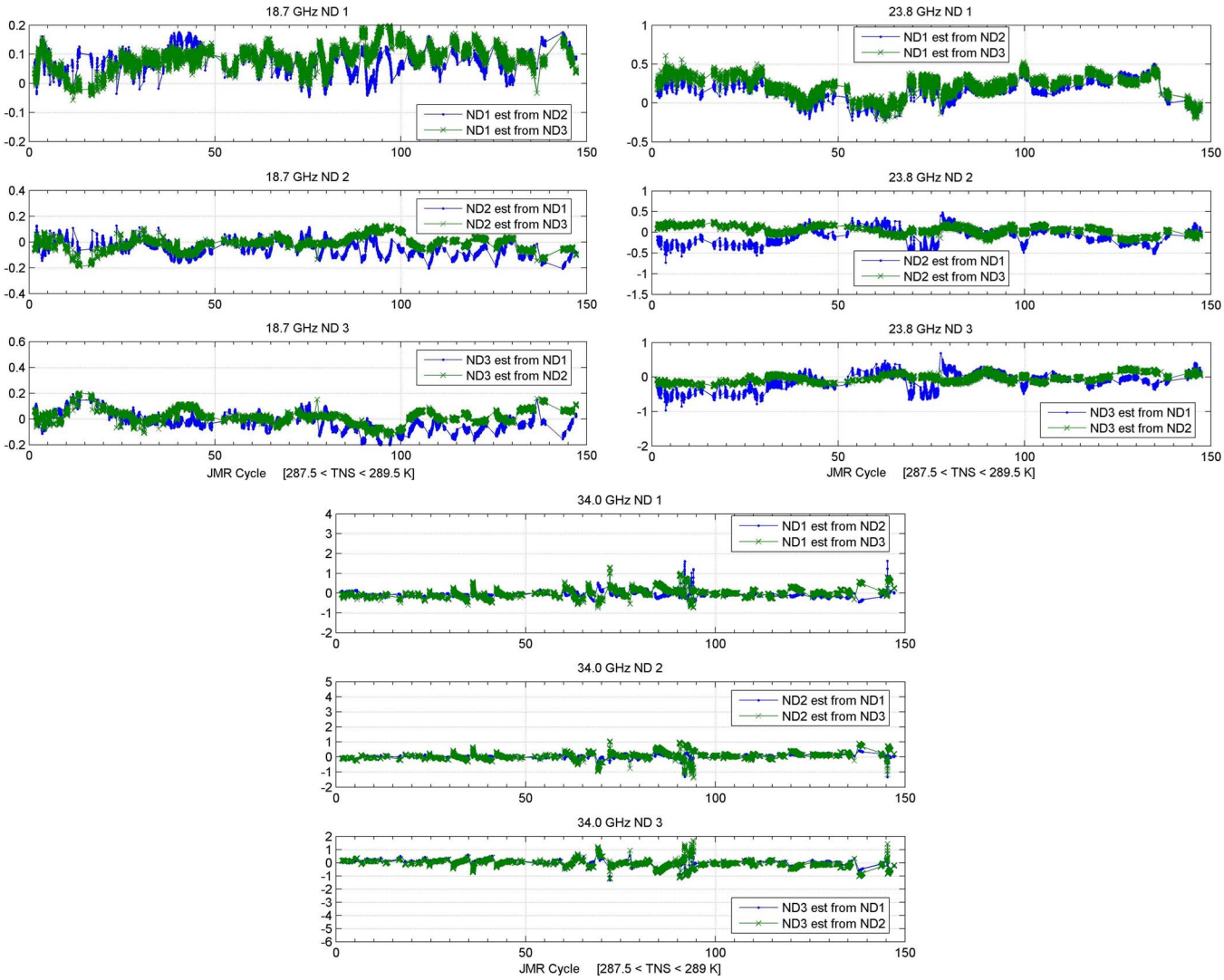

Fig. 12. Δ_{ND}^{j} for the different combinations of the three NDs using the derived T_{ND0} time series at (top left) 18.7, (top right) 23.8, and (bottom) 34.0 GHz. These plots are for a physical ND temperature of 288.5 + 1.0 K. The y axis is expressed in Kelvin.

Fig. 15. The absolute change in ND brightness is shown in the left ordinate, and the percent change from the initial value is shown on the right ordinate.

The AWVR NDs are demonstrating a similar level of stability as the JMR diodes. Some diodes are stable to better than 0.5% over the four-year time period, whereas others drift considerably. As with JMR, the 31.4-GHz diodes show more instability than the 22.2- and 23.8-GHz diodes. This fact provides an important clue as to the mechanism for the instability and is discussed further in the next section. The 31.4-GHz ND B on A1 decreases by about 3% over the four years. The A1 22.2- and 23.8-GHz ND A drift by about 1% and 2%, respectively. The A2 23.8-GHz diodes are each stable to better than 0.5% over the four years. The 22.2-GHz diodes on A2 show similar stability, with the exception of a 0.75% jump in ND C. The 31.4-GHz diodes on A2 show much more instability. The A2 31.4-GHz ND B drops by nearly 2% around day 800 and then recovers. A hardware change was made to the A2 31.4-GHz ND C after day 1300, which changed its effective brightness. Before this, the diode brightness decreased by about 2%. The data after the hardware change is not shown in the plot.

VII. Discussion

Instability of the ND effective brightness can be caused by changes in the output of the diode itself, which in turn can be caused by changes in the bias current driving the diode among other things or changes in the ohmic and reactive losses of the components between the diode and the receiver. We can use the circumstantial evidence from the JMR and AWVR, along with previous laboratory experience [15], to conjecture on which is more likely to cause the observed instability. If the instability was in the diode itself, then it is expected that the diode trends would be common to the shared channels, which was not observed. One could advance the argument that the changes in diode output may be frequency dependent, making this assumption invalid, but given the close proximity of the frequencies involved (especially the 22.2- and 23.8-GHz channels of AWVR), this is not believed to be the case. More likely, it is changes in the impedance mismatches between components in the ND circuit that modify the finite reflections at the component interfaces, thus inducing a change in the detected signal. Similarly, because of the finite directivity of the ND coupler,

TABLE III
(a) RMS OF $\Delta T_{\mathrm{ND}}^{j}$ BEFORE RECALIBRATION. (b) RMS OF $\Delta T_{\mathrm{ND}}^{j}$ AFTER RECALIBRATION

(a)

Channel	ND1	ND2	ND3
18.7 GHz	0.04 K	0.10 K	0.10 K
23.8 GHz	0.39 K	0.06 K	0.06 K
34.0 GHz	0.41 K	0.76 K	0.90 K

(b)

Channel	ND1	ND2	ND3
18.7 GHz	0.06 K	0.04 K	0.04 K
23.8 GHz	0.14 K	0.08 K	0.08 K
34.0 GHz	0.10 K	0.17 K	0.21 K

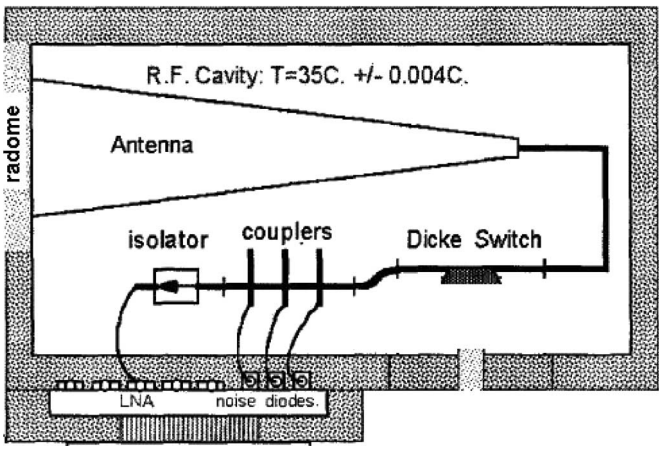

Fig. 13. Simplified block diagram of the AWVR in its temperature enclosure.

any change in front-end mismatches will also effect the ND brightness. It is expected that front-end changes will introduce common-mode variations among the diodes. The mechanism for this type of change is associated with component aging and/or temperature shock. Both of these effects are in play for JMR, but only the former is in play for AWVR. This may also explain why the ND brightness shows more instability for the higher frequency channels for both JMR and AWVR. Thermal forcings and aging cause dimensional changes in components, such as the expansion and contraction of the Teflon dielectric in the coaxial transmission line. A small dimensional change relative to the wavelength will have a larger effect to millimeter-wave circuits, as compared to centimeter-wave ones.

The observed long-term stability of the JMR and AWVR NDs suggest that a single ND can only be relied on for long-term calibration stability to the 2%–3% level. This statement is qualified for diodes operating near the range of 18–40 GHz with coaxial transmission lines, as the coaxial lines are thought to be the leading candidate for the instability mechanism previously described. In the absence of external recalibration, the addition of redundant diodes should improve overall stability since some diodes are observed to be stable to the 0.5% level. If the NDs are routinely recalibrated through other means, whether it be on-Earth references for the satellite case or tip-curve

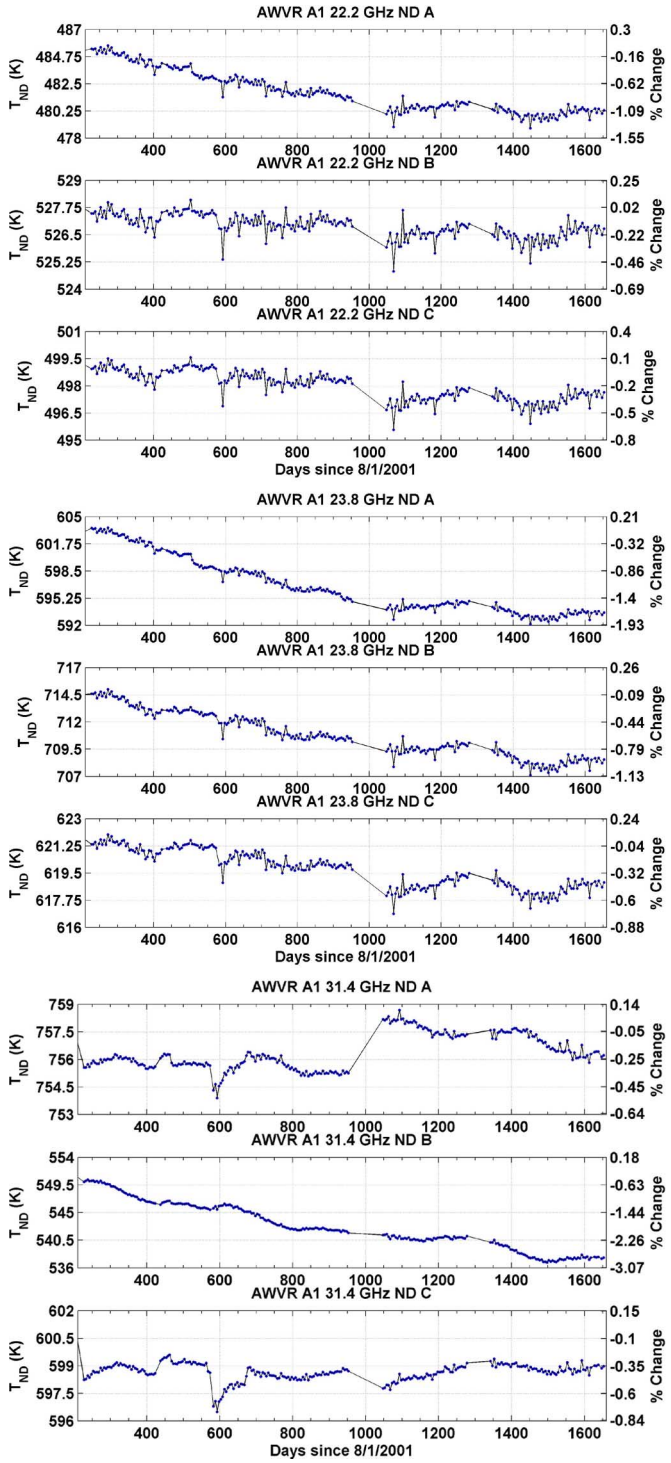

Fig. 14. AWVR A1 ND brightness from August 2001 to July 2005 at (top) 22, (middle) 23.8, and (bottom) 31.4 GHz. The percent deviation from the initial value is given on the right axis.

calibrations for the ground-based case, they can be relied on to monitor short-term gain fluctuations. In the case of the JMR, the methodology presented here demonstrates that long-term stability can be achieved with frequent ND monitoring and recalibration. The long-term PD slope error was reduced from 3.9 to -0.01 mm/year. The T_{B} stability achieved over a ten-day averaging window is estimated to be at 0.25 K.

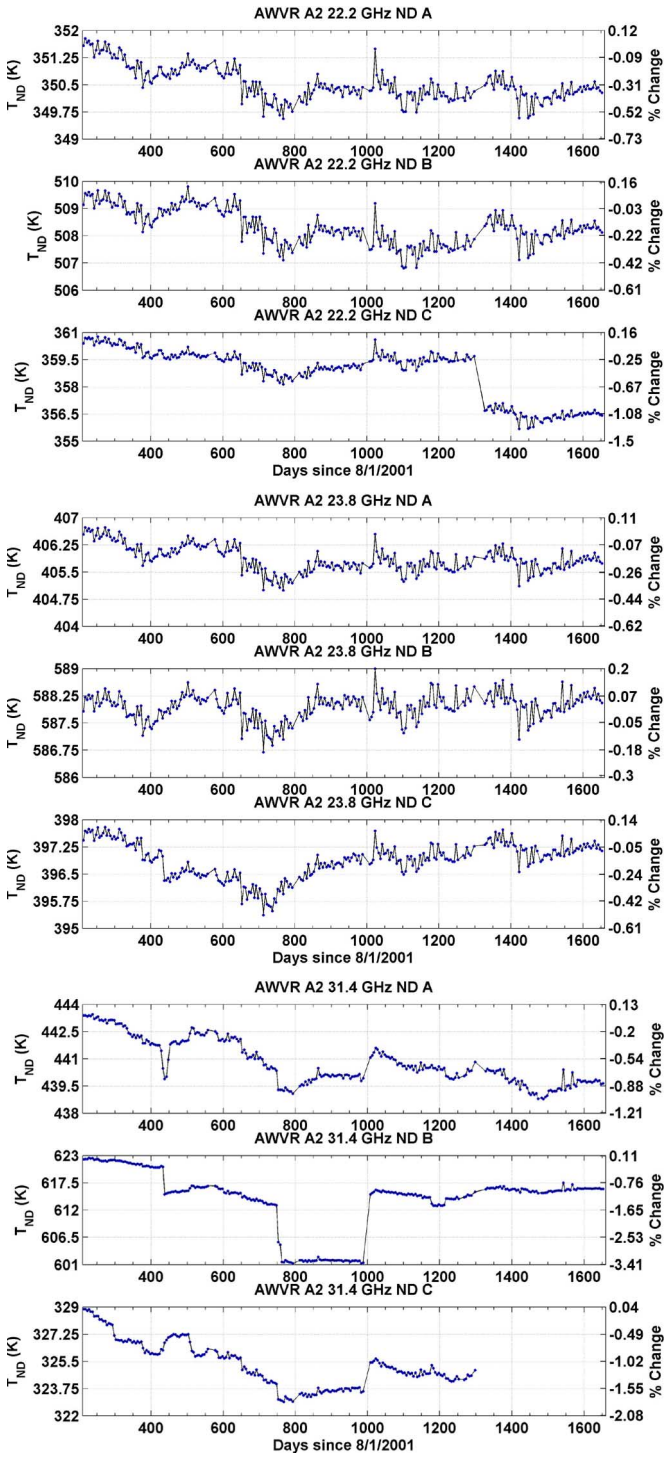

Fig. 15. AWVR A2 ND brightness from August 2001 to July 2005 at (top) 22, (middle) 23.8, and (bottom) 31.4 GHz. The percent deviation from the initial value is given on right axis.

A rigorous discussion on radiometer design for satellite microwave radiometers, which use internal calibration, is beyond the scope of this paper, but a short discussion is merited. Calibration instability is inherent to radiometers that use internal references, regardless of whether these references are NDs. For example, the TMR 18.0-GHz channel, which is calibrated using an internal switch to a cold sky horn, is observed to drift by about 1.5 K over the period of seven years [17]. The other TMR channels drift by less than 0.5 K over 13 years. JMR is the first satellite radiometer to use NDs for calibration, and the experience with this radiometer has led to some design changes to the ND circuit for the JMR follow-on AMR and changes to the prelaunch testing and qualification. The AMR ND circuits are an all-microstrip design, eliminating the known instabilities associated with coaxial transmission lines. In addition, the AMR noise source units, both separately and integrated with the instrument, are submitted to an extended burn-in period and repeated thermal shocks. This stems from the observation that most of the JMR instabilities have occurred after instrument safehold events where there is a large thermal shock to the instrument.

VIII. Conclusion and Future Work

The four-year ND time history was presented for the ground-based AWVR and the JMR, which is the first radiometer to be flown in space that uses NDs for calibration. The ND brightness was derived using external calibration techniques. Continuous tip curves were used to monitor the ND brightness of the AWVR channels. Stable on-Earth hot and cold references were used to monitor the JMR diodes. An optimal estimation-based calibration system was developed to estimate the set of calibration coefficients that minimize the rms difference between the JMR T_{B}s and on-Earth hot and cold references. The calibration system was used to derive a time series of the JMR ND effective brightness temperature.

It was determined that adjusting the ND brightness alone for the JMR 23.8- and 34.0-GHz channels was not able to minimize the rms difference between the JMR and the on-Earth references over the first four years of the mission. For these channels, both the ND brightness and a front-end path loss coefficient were adjusted. It is shown that these time variable coefficients remove the jumps in the PD retrievals and significantly reduce the relative changes between the diodes.

Both the JMR and AWVR diodes showed various levels of instability over the four-year time period, ranging from 0.2% to 3%. Even though two of the JMR channels and all the AWVR channels share NDs, the observed changes were not correlated among the channels for a given shared diode. This suggests that the instability is associated with the ND circuit and not the ND itself. Small changes in reflections at component interfaces could cause the observed instability. These changes could result from component aging or thermal shock.

The methodology presented for the recalibration and monitoring of the JMR NDs could be used for future spaceborne radiometers, which will use NDs for calibration, assuming stable on-Earth references can be found for the given radiometer frequency (e.g., at L-band, Antarctic ice sheets will likely replace the Amazon as a stable hot target). The current methodology used a stable hot and cold on-Earth T_{B} reference. As the reliability of the retrieved coefficients is directly related to the random and systematic errors present in the on-Earth references, improvements could be made by including and developing other independent T_{B} references. Examples that have been used for previous on-orbit calibration campaigns include comparisons to modeled T_{B}'s from numerical weather

prediction analysis fields or comparisons with upward looking radiometers. It is also expected that improving the way the coefficients are assimilated into the processing software (i.e., smoothing, interpolating, etc.) will aide in reducing the calibration instability. This includes finding the optimum recalibration time window where the instability of the radiometer and the statistical uncertainty of the on-Earth references balance, thereby removing the long-term trends while introducing a minimum level of additional short-term noise. These areas will be the focus of a future investigation in preparation for the postlaunch monitoring of the AMR on Jason-2, which is functionally equivalent to the JMR, but with an improved ND circuit design.

REFERENCES

[1] J. Hollinger, J. Peirce, and G. Poe, "SSM/I instrument evaluation," *IEEE Trans. Geosci. Remote Sens.*, vol. 28, no. 5, pp. 781–790, Sep. 1990.

[2] C. Kummerow, W. Barnes, T. Kozu, J. Shiue, and J. Simpson, "The Tropical Rainfall Measuring Mission (TRMM) sensor package," *J. Atmos. Ocean. Technol.*, vol. 15, no. 3, pp. 809–817, Jun. 1998.

[3] P. Gaiser *et al.*, "The WindSat spaceborne polarimetric microwave radiometer: Sensor description and early orbit performance," *IEEE Trans. Geosci. Remote Sens.*, vol. 42, no. 11, pp. 2347–2361, Nov. 2004.

[4] C. Ruf, S. Keihm, and M. Janssen, "TOPEX/Poseidon Microwave Radiometer (TMR)—Part I: Instrument description and antenna temperature calibration," *IEEE Trans. Geosci. Remote Sens.*, vol. 33, no. 1, pp. 125–137, Jan. 1995.

[5] S. Brown, C. Ruf, S. Keihm, and A. Kitiyakara, "Jason Microwave Radiometer performance and on-orbit calibration," *Mar. Geod.*, vol. 27, no. 1, pp. 199–220, 2004.

[6] E. W. Leuliette, R. S. Nerem, and G. T. Mitchum, "Calibration of Topex/Poseidon and Jason altimeter data to construct a continuous record of mean sea level change," *Mar. Geod.*, vol. 27, no. 1/2, pp. 79–94, 2004.

[7] A. Tanner and A. Riley, "Design and performance of a high stability water vapor radiometer," *Radio Sci.*, vol. 38, no. 3, pp. 15.1–15.12, Mar. 2003.

[8] W. Wilson, S. Yueh, S. Dinardo, and F. Li, "High-stability L-band radiometer measurements of saltwater," *IEEE Trans. Geosci. Remote Sens*, vol. 42, no. 9, pp. 1829–1835, Sep. 2004.

[9] M. A. Janssen, M. D. Hofstadter, S. Gulkis, A. P. Ingersoll, M. Allison, S. J. Bolton, S. M. Levin, and L. A. Kamp, "Microwave remote sensing of Jupiter's atmosphere from an orbiting spacecraft," *Icarus*, vol. 173, no. 2, pp. 447–453, Feb. 2005.

[10] C. Ruf, "Detection of calibration drifts in spaceborne microwave radiometers using a vicarious cold reference," *IEEE Trans. Geosci. Remote Sens.*, vol. 38, no. 1, pp. 44–52, Jan. 2000.

[11] S. Brown and C. Ruf, "Determination of an amazon hot reference target for the on-orbit calibration of microwave radiometers," *J. Atmos. Ocean. Sci.*, vol. 22, no. 9, pp. 1340–1352, 2005.

[12] S. Desai and B. Haines, "Monitoring measurements from the Jason-2 Microwave Radiometer and independent validation with GPS," *Mar. Geod.*, vol. 27, no. 1, pp. 221–240, 2004.

[13] V. Zlotnicki and S. Desai, "Assessment of the Jason Microwave Radiometer's measurement of wet tropospheric path delay using comparisons to SSM/I and TMI," *Mar. Geod.*, vol. 27, no. 1, pp. 241–253, 2004.

[14] C. Rodgers, "Inverse methods for atmospheric sounding," in *Theory and Practice*. River Edge, NJ: World Scientific, 2000, pp. 83–853.

[15] A. Tanner, "Development of a high stability water vapor radiometer," *Radio Sci.*, vol. 33, no. 2, pp. 449–462, Mar./Apr. 1998.

[16] M. A. Janssen, *Atmospheric Remote Sensing by Microwave Radiometry*. New York: Wiley, 1993.

[17] R. Scharroo, J. Lillibridge, and W. Smith, "Cross-calibration and long-term monitoring of the microwave radiometers of ERS, TOPEX, GFO, Jason, and Envisat," *Mar. Geod.*, vol. 27, no. 1, pp. 279–297, 2004.

Shannon T. Brown (S'02–M'05) received the B.S. degree in meteorology from Pennsylvania State University, University Park, and the M.S. and Ph.D. degrees, in 2005, from the University of Michigan (UMich), Ann Arbor.

In 2005, he joined the Microwave Advanced Systems Section, NASA Jet Propulsion Laboratory, Pasadena, CA, as a member of the engineering staff. He has also been involved with the spaceborne Topex and Jason Microwave Radiometers, the WindSat Polarimetric Radiometer, and the Jason follow-on Advanced Microwave Radiometer. His research interests include microwave radiometer calibration, geophysical algorithm development for both passive and active sensors, and cloud and precipitation science.

Dr. Brown was a recipient of the NASA Group Achievement Award in 2004 for his contribution to the UMich/Goddard Space Flight Center Lightweight Rainfall Radiometer.

Shailen Desai received the B.S. degree in aeronautical and astronautical engineering from Purdue University, West Lafayette, IN, in 1990, and the M.S. and Ph.D. degrees in aerospace engineering sciences from the University of Colorado, Boulder, in 1992 and 1996, respectively.

In 1996, he joined the engineering staff in the Ground-Based Microwave Applications Group, Jet Propulsion Laboratory (JPL), Pasadena, CA. His work at JPL has included the development of software for the autonomous optical navigation system on the Deep Space-1 mission, the development of global ocean tide models from satellite altimetry, the application of ocean tides to Earth rotation, the calibration and validation of the sea surface height measurement systems on the Topex/Poseidon and Jason-1 satellite altimeter mission, various geodetic applications from terrestrial GPS sites, and GPS-based orbit determination of the Jason-1 mission. He is a Principal Investigator and Coinvestigator of the Ocean Surface Topography Science Team, a Principal Investigator of NASA's Solid Earth and Natural Hazards Program, and has been a Coinvestigator of NASA's Oceanography Program.

Dr. Desai is a member of the American Institute of Aeronautics and Astronautics and American Geophysical Union.

Wenwen Lu received the B.S. degree from Fudan University, Shanghai, China, and the Ph.D. degree in high-energy physics from the California Institute of Technology, Pasadena.

In 1997, she joined the Mission Simulation and Instrument Modeling Group, NASA Jet Propulsion Laboratory, Pasadena, CA. In 2004, she joined the Orbit and Radio Metric Systems Group, NASA Jet Propulsion Laboratory, where she is currently a Senior Engineer, supporting three tasks in the calibration and validation of the Topex and Jason microwave radiometers projects, namely recalibration of the Jason-1 Microwave Radiometer, recalibration of the Topex Microwave Radiometer, and data evaluation, verification, and monitoring of both Jason and Topex Microwave Radiometers using GPS, SSM/I, and TMI.

Alan B. Tanner received the B.S. and Ph.D. degrees from the University of Massachusetts, Amherst, in 1984 and 1989, respectively.

He is currently a Microwave Systems Engineer in the Ground-Based Microwave Applications Group, Jet Propulsion Laboratory (JPL), Pasadena, CA. His work at JPL has focused on the design and calibration of radiometers and radar scatterometers for remote sensing.